2024-01-2703

Exhaust Slip-Stream Sampling System for Aftertreatment Device Testing

Jason Loprete, Rodrigo Ristow Hadlich, Amanda Sirna, Dimitris Assanis
Department of Mechanical Engineering, Stony Brook University, New York, USA

Tala Mon, Eleni Kyriakidou
Department of Chemical and Biological Engineering, University of Buffalo, New York, USA

Abstract

Design, testing, and implementation of new aftertreatment devices under various engine operating conditions is necessary to meet increasingly stringent regulatory mandates. One common aftertreatment device, the catalytic converter, is typically developed at a reduced scale and tested using predefined fluid compositions sourced from bottle gases and can undergo both species and temperature cycling in addition to steady-state testing. However, these bench-top conditions may differ from real-world operation in terms of flow-rates, species composition, and temperatures experienced. Transitioning from small-scale bench-top testing to full-scale engine applications requires larger monoliths that therefore have a significant amount of catalyst slurry to be washcoated, which increases cost and fabrication time. Being able to experience realistic emission streams under scaled flowrates would allow for a physically smaller catalyst testing at matched space velocities resulting in faster, more cost-effective determination of aftertreatment device effectiveness. This work documents the design and performance of an intermediary-scale (5-50 SLPM) setup to aid in the catalyst testing process. This is accomplished using a secondary exhaust branch to flow a variable percentage of exhaust from the main branch. The system siphons exhaust via a slip-stream approach driven by a venturi ejector, which is commonly used in automotive applications to dilute samples for emissions analysis. Instead, the pre-diluted flow from the ejector is routed through the catalyst, where post catalyst emissions testing occurs. The system is evaluated under a range of engine operating conditions with varied equivalence ratio and intake pressures to affect exhaust out temperatures / catalyst inlet temperature which is critical for testing catalyst activation. Emissions are recorded in both the main and secondary branch with no aftertreatment device installed to verify compositional parity. Initial results show that the two branches produce self-similar engine-out emissions, but with the ability to scale flow and modulate temperature through the secondary catalyst testing branch.

Introduction

Reducing greenhouse gas emissions is a focus of many nations across the globe with time-sensitive target goals [1, 2]. While many pathways exist to achieve these goals, aftertreatment devices are one approach to meet increasingly strict emissions regulations [3, 4]. In particular, one form of aftertreatment, the use of catalysts, plays an important role in automotive exhaust aftertreatment in both spark ignition and compression ignition engines [5–9]. Development of catalytic converters for automotive applications consists of synthesizing the catalyst material, generating a support structure (typically a honeycomb monolith), washcoating of the catalyst material onto the substrate, drying, and calcining at elevated temperatures [10, 11]. Pre-pilot benchtop testing often begins using a small-scale washcoated monolith (mini-core) to evaluate the conversion efficiency of the resulting catalyst and perform physiochemical and structural characterization. Once an optimal configuration is determined, the catalyst is scaled up for full scale testing under real flow conditions to determine deterioration and real performance characteristics. These flow conditions are traditionally generated either using simulated drive-cycles with gas bottles [12] or with physical engine exhaust [13, 14]. Scaling up of the catalyst has practical challenges: more catalyst precursor material is required, as well as additional fabrication and curing time. Full-scale engine tests thus become time and cost-prohibitive [15] and alternatives to simulate this process have been performed, such as using hot air and the desired pollutant to simulate real exhaust gas [16]. Furthermore, additional considerations have to be made regarding changes in gas and particle kinetics, operating temperatures, and chemical composition [17]. Full-scale testing thus incorporates an inherent risk in terms of time and material investment. A solution to this in intermediate scaling, where the catalyst is sized up to a fraction of the full-scale size with matched composition, temperature, and flow requirements. Intermediate scaling can be difficult, as without additional instrumentation, flow conditions through the catalyst are determined solely by the species generating appliance's operating conditions. Desired species may be generated at one operating point, but produce incompatible flowrates with the intermediately-sized catalyst. Two main approaches have been explored in the literature: the usage of a catalyst bypass to redirect any undesired exhaust flow away from the catalyst [18], or a vacuum-pump powered slip-stream to siphon a portion of exhaust flow [19]. These approaches can be further improved to create a more generalized approach to decouple the generating appliance's outlet flow from the flow entering the catalyst, and instead allow for a variable scaled-down realistic flow stream to be utilized.

This study focuses on the development and validation of an exhaust sampling system that draws a portion of the main exhaust flow directly into the catalyst, allowing for realistic engine conditions to be tested at an intermediate scale. Specific parameters relevant to catalyst testing are defined and discussed. Methods of siphoning the secondary flow stream to the catalyst are introduced and evaluated. The design of the system is discussed in detail, with the system's capabilities in terms of operating temperatures and emissions species compared to that of the main exhaust branch.

Representative Sampling and Scaling Considerations

The secondary exhaust branch will be taking a sample of exhaust gases from the main exhaust stream to flow through the catalyst. The main challenge with this approach is determining if the smaller sample of

exhaust flow is representative of the composition of the main exhaust. The way the sample is taken can introduce unknown biases for certain species and possible particulate matter sampling and thus the condition of the flows and their speeds need to be considered. If the flow through the main exhaust runner is well mixed and there is no compositional stratification, the sample taken will not be biased to certain gaseous species and is representative of the main flow. In order for the flow to be well mixed inside the exhaust runner, the flow inside the runner must be turbulent [20]. To determine whether or not the flow is turbulent, the Reynolds number can be used according to Eq. (1):

$$Re = \frac{\rho V D}{\mu} \tag{1}$$

where the characteristic length, D, is defined to be the inner diameter of the main exhaust runner (31.75 mm); the average velocity, V, is determined from an estimated volume flow rate from conservation of mass between intake and exhaust using the cross sectional area of the main exhaust runner (14.4 m/s); the density, ρ, in the exhaust was found by combining the densities of the assumed exhaust species on a mole fraction basis; the dynamic viscosity, μ, was found by combining viscosities of exhaust species on a mole fraction basis [21]. The chemical composition of the exhaust species is assumed to be the products of the complete combustion of our primary test fuel, methane, as depicted in Eq. (2).

$$CH_4 + 2(O_2 + 3.76N_2) \rightarrow CO_2 + 2H_2O + 7.52N_2 \tag{2}$$

With the mole fractions, y_i, determined via Eq. (2), an effective density and effective viscosity of the exhaust was calculated using Eq. (3) and Eq. (4), respectively.

$$\rho_{exh} = \sum_{i=1}^{n} y_i \rho_i \tag{3}$$

$$\mu_{exh} = \sum_{i=1}^{n} y_i \mu_i [21] \tag{4}$$

The Reynolds number for the gas mixture flowing through the exhaust runner was found to be 4767.7 when evaluated using fluid properties at 600 °C, which is the upper limit of the temperatures investigated in this study. This temperature exceeds the activation range for several catalyst washcoat compositions commonly used in three-way catalyst applications [22], and a decrease in temperature will only result in an increase in the Reynolds number and sufficient turbulence due to temperature's effect on the density and viscosity of gases. Traditionally, the critical Reynolds number for the transition from laminar to turbulent flow in a circular pipe is 2300, though the presence of perturbations and pulsating flow can reduce this requirement significantly [23] such that the stated value exceeds this threshold. Due to the pulsating nature of the flow as a result of the opening and closing of the exhaust valve creating such perturbations, and the turbulent mixing within the combustion chamber, it can be assumed that the flow within the exhaust runner is turbulent and well-mixed. Turbulence is often used as an indicator of complete mixing [20], and thus can provide confidence that the gaseous sampling is unbiased.

Gases are representatively sampled regardless of sample velocity [24], but this behavior is not true for particulate matter, which is present in many combustion exhaust streams. It is of note that the current species generating application, spark-ignition combustion, produces little particulates [25] compared to diesel exhaust or biomass combustion, but the analysis is included to extend the use of the system to more general operation where particulate production is more prominent. The representative sampling of particulates can be broken down into three

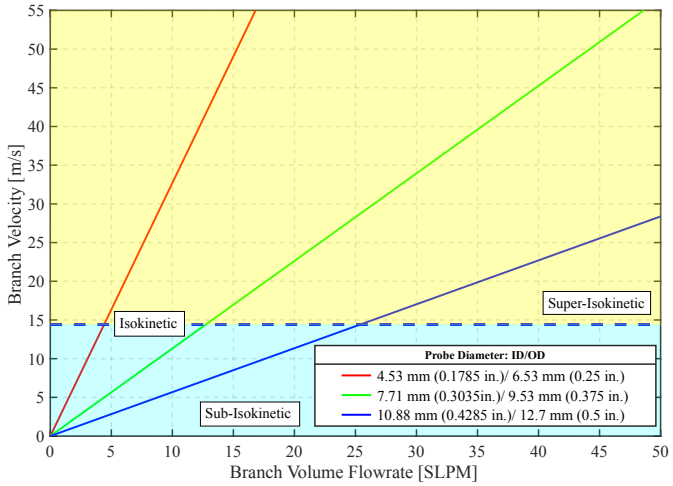

Figure 1: Branch velocity as a function of branch volume flowrate for common tubing diameters, with sub-isokinetic (blue), super-isokinetic (yellow), and isokinetic (dashed line) regions identified based on main exhaust velocity.

categories: super-isokinetic, isokinetic and sub-isokinetic, with the determining variable being the velocity of the secondary flow compared to the primary flow [24]. Super-isokinetic sampling is when the velocity of the sample flow is greater than the velocity of the main flow. This increased velocity in the probe means that larger particulates can be under sampled due to their inertial forces. Sub-isokinetic sampling is when the velocity in the probe is less than the velocity in the main flow and the inertia of the larger particles causes them to be over sampled. In both of these sampling conditions, there is a bias that will be associated with the size distribution of particulates. For the isokinetic category, the velocity in the probe and in the main flow are equal [24]. This allows for the main flow to remain undisturbed from the probe and an accurate representative sample can be taken free of bias [26]. Figure 1 shows how the volumetric flowrate and the diameter of the tubing used for the secondary branch can affect what category of sampling occurring at a constant exhaust flow. Depending on the application of this secondary branch, different diameters and volumetric flowrates can be selected to accurately sample the main exhaust. If the branch flowrate is fixed and a particular sampling condition must be met, such as isokinetic sampling, a probe of different diameter can be used to meet this condition. Similarly, if the probe diameter must be fixed, the flowrate can be adjusted to meet the required sampling condition. For the application used in this study, as no particulates are expected in the exhaust gases, a constant 6.35 mm (1/4") tubing was used. While the majority of operating conditions will produce super-isokinetic sampling for this size tubing, the lack of particulates for the application in question negates any bias that would otherwise occur. As the majority of the operating conditions for the 6.35 mm (1/4") tubing are super-isokinetic, this set up would not be appropriate for a diesel fuel combustion in a compression ignition engine, as this combustion mode is known to produce more particulate matter. In general, the sampling probe diameter at the secondary branch inlet can be adjusted to acquire the desired flow condition and maintain isokinetic sampling where necessary.

Catalyst Scaling Considerations

Scaling-up powdered catalysts to washcoated monoliths requires a scaling factor, e.g., space velocity, volumetric flow rate of reactants per catalyst amount (mass or volume) [27]. The catalyst weight is used for calculating the weight hourly space velocity ($WHSV$) that is primarily used for powdered catalysts, while the catalyst volume is used for calculating the gas hourly space velocity ($GHSV$) for monolith performance evaluations:

$$GHSV = \frac{\dot{V}}{V_{monolith}} \tag{5}$$

Table 1: Scale up of washcoated monolith with exhaust flow of 50 standard liters per minute (SLPM defined at standard temperature and pressure (STP at 0 °C and 1 bar)) and a washcoat loading of 61 g L^{-1} (1 g in^{-3}) (95 wt.% catalyst and 5 wt.% binder)

GHSV [h^{-1}]	CH4 conversion [%]	Monolith volume [L]	Washcoat loading [g]	Catalyst weight [g]
30,000	100	0.100	6.10	5.80
60,000	100	0.050	3.05	2.90
120,000	50	0.025	1.53	1.45

where $\dot{V}$ is the volumetric flow rate and $V_{monolith}$ is the monolith volume. The $GHSV$ is preferred for comparing the performance of different catalysts since it is taking into consideration catalyst density differences. The wide range of GHSVs (8,000-110,000 h^{-1}) for methane (CH_4) abatement reported in literature, led the USDRIVE advanced combustion and emissions control team to standardize the $GHSV$ used in the low temperature oxidation catalyst test protocol to 30,000 h^{-1} [27–29]. An optional higher $GHSV$ of 60,000 h^{-1} is also proposed by USDRIVE for heavy-duty engines when scaling from powdered catalysts to washcoated monoliths.

Scaling up powdered catalysts to washcoated monoliths results to a lower pressure drop as the feed gas is not forced to flow through the powdered catalyst but it rather flows through the monolith channels and reacts with the washcoated walls [30, 31]. The benefit of the low pressure drop observed over washcoated monoliths comes at the cost of limited mass transfer in the form of external (bulk gas to catalyst surface) and internal (catalyst surface to pores) diffusion limitations at high flow rates (i.e., high $GHSV$s). High $GHSV$s typically result in mass transfer limitations leading to increased temperatures required to achieve similar conversions as lower $GHSV$s over a fixed monolith volume. For example, increasing the $GHSV$ from 30,000 to 575,000 h^{-1} over a Platinum on alumina (Pt/Al_2O_3)-coated monolith resulted in an increase in the temperature required to achieve 50% carbon monoxide (CO) conversion from 150 to 240 °C [32]. In addition, CO conversion plateaus at 70% for $GHSV$s > 30,000 h^{-1}, indicating that the reaction has become mass transfer limited. Thus, the $GHSV$ should be optimized to determine when the reaction becomes mass transfer limited to properly size a monolith for scale up. Table 1 shows an example where a catalyst reaches 100% CH_4 conversion at $GHSV$s of 30,000, 60,000 h^{-1} and 50% CH_4 conversion at $GHSV$ of 120,000 h^{-1} due to mass transfer limitations. $GHSV$s of 30,000 and 60,000 h^{-1} with no mass transfer limitations were considered for sizing a monolith for scale up. The calculated monolith volume and required catalyst weight decrease from 0.1 L/5.8 g to 0.05 L/2.9 g with increasing $GHSV$ from 30,000 to 60,000 h^{-1}.

To further minimize the monolith volume and catalyst weight, the catalyst must be able to achieve 100% CH_4 conversion at $GHSV$s > 60,000 h^{-1} based on the example provided previously. Developing such a monolithic catalyst requires decreasing the effect of mass transfer limitation in the form of internal and external diffusion limitations by altering the washcoated monolith properties such as washcoat loading and the monolith cell density [33]. Increasing washcoat loading can improve performance; however, higher loading may lead to higher pressure drop due to restriction of the flow by the increasing thickness of washcoat within the cells and limiting internal diffusion. The impact of the internal diffusion limitation can be quantified by comparing the ratio of the reaction rate at the catalyst surface and the reaction rate inside the catalyst (internal effectiveness factor). Internal effectiveness factor of 1 signifies no internal diffusion limitations and < 1 indicates that internal diffusion limitations have some control over the reaction rate. For instance, Vergunst et al. showed that increasing the monolith washcoat thickness from 20 to 140 µm for the selective hydrogenation of phenylacetylene led to a decrease of the catalyst internal effectiveness factor from 0.95 to 0.30 indicating that the increase in the washcoat thickness limited the internal diffusion of the reactants within the catalyst [34]. Optimization is also required for the monolith cell density to maximize external diffusion, since high monolith cell density leads to a high surface area to volume ratio. The external effectiveness factor can quantify external mass diffusion limitations by using the ratio of the bulk reaction rate and the reaction rate at the catalyst surface. Thus, increasing the cells per square inch from 200 to 11000 led to an increase in the external effectiveness factor from 0.91 to 0.96 indicating that a higher cell density allows more of the reactants to reach the catalyst surface leading to decreased external diffusion limitations. By addressing the causes of mass transfer limitations in washcoated monoliths through minimization of washcoat thickness and optimization of cell density, higher $GHSV$s (e.g. 120,000 h^{-1}) can be used, leading to smaller monolith volumes and decreased catalyst usage in the process of scaling up a powdered catalyst to a monolith.

Engine Facility Specifications

The secondary branch and sampling system were integrated into an existing experimental setup described in detail in previous works, where additional information is available regarding previous emissions studies and uncertainty quantification [35–37]. The setup has been used to test different fuels relevant to catalyst development [38], which helps to understand the range of exhaust temperatures and species the system is capable of producing. The research group has also been investigating the usage of hydrogen to enhance combustion performance and increase burning speeds, which may shorten combustion duration and be phased to increase exhaust temperatures [39]. Furthermore, alternative ignition methods beyond spark ignition have been investigated, such as a retrofitted spark plug replacement pre-chamber, with the change in combustion performance being an additional control parameter to generate different exhaust gas conditions in terms of both temperature and constituents [40]. In essence, a single-cylinder spark-ignited Cooperative Fuel Research (CFR) engine was utilized to generate the realistic engine flows and compositions to be sampled over a variety of operating conditions. K-type thermocouples were used to measure system temperatures, and a HORIBA MEXA 7100D was used to measure exhaust emissions species. A detailed schematic of the instrumented setup is included in Figure 2. Critical measurements such as air and fuel flowrates, intake and cylinder pressures, system temperatures, crankshaft position, and emissions species were recorded utilizing a National Instruments cDAQ and a custom built LabVIEW program. Data is then post-processed and visualized in MATLAB to exhibit the range of the system's capabilities.

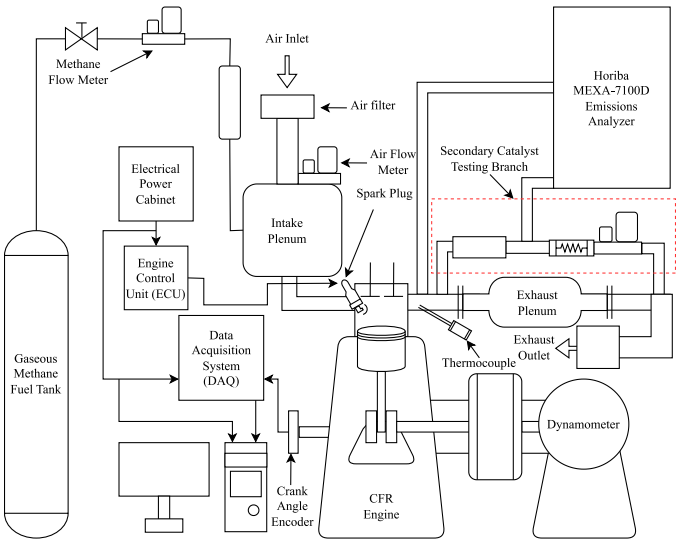

Figure 2: Schematic of experimental facility.

Secondary Branch Development

The secondary branch must be able to meet the aforementioned sampling and scaling requirements, as well as meet the activation temperature range for the catalyst. Different catalysts have different activation temperatures, and thus the system must be able to provide a range of catalyst inlet temperatures to suit specific installation needs. Several factors impact the temperature at the inlet of the catalyst and flow conditions, described in detail in the following subsections.

Secondary Branch Geometric Characteristics

The length of the sampling branch and the surface-area-to-volume ratio are critical factors that affect the total amount of heat lost, and thus the temperature, prior to the sample stream entering the catalyst. A longer pre-catalyst length results in a lower average temperature entering the catalyst, and a larger diameter tube results in less effective heat transfer to the surroundings (a higher catalyst inlet temperature). Thus, portions of the line can be replaced according to these two factors if a different temperature range is required. The heat lost in the sampling line can be determined empirically through the use of thermocouples embedded in the flow stream at two locations along the sampling path. The rate of heat loss per unit length, $\dot{q}_{loss}$, is then determined via Eq. (6),

$$\dot{q_{loss}} = \frac{\rho \dot{V} c_p (T_{in} - T_{out})}{L} \tag{6}$$

where ρ is the density, $\dot{V}$ is the volume flow rate through the catalyst, c_p is the specific heat at constant pressure, L is the sampling section length, and T_{in}/T_{out} are the temperatures at the inlet and outlet of the sampling section, respectively. Note that while the heat lost is sensitive to sample composition and flow rate, all that is needed is the extremes of the operating range (lean to rich combustion exhaust products) to determine an estimate for heat loss in this way. This amount of heat loss can then be used for additional components, such as heat tape, that may be required as an additional experimental parameter to vary the catalyst inlet temperature. In practice, the resulting temperature gradient along the length of the tube can be used at different flow conditions. Preliminary testing with 6.35 mm (1/4") stainless steel tubing results in an initial temperature gradient of approximately 4.92 °C/cm (150 °C/ft) of tubing at the branch system inlet, which makes the use of additional length and location of the catalyst a significant tuning parameter.

Siphoning the Secondary Flow

There are several approaches to siphoning a secondary flow stream from the main exhaust branch. One common approach is through the use of a vacuum pump; however, there are several challenges associated with the use of such systems in undiluted exhaust gas sampling. If flow scaling is required, a single stage vacuum pump will only be able to pull a fixed flow without additional components. Variable speed drive vacuum pumps are an alternative option, but are typically more costly. Furthermore, the presence of particulates in the exhaust stream and potential unburned fuel can possibly damage the pump's internals, which requires the use of additional filters to protect the equipment. Lastly, the devices are prone to overheating during continuous operation (common for steady-state engine testing), which requires the installation of a cooling system to prevent system failure.

Instead, this work utilizes a venturi ejector driven by compressed air to siphon the flow. Venturi ejectors are already commonly used in automotive applications to dilute exhaust gas [41–44], making them suitable when particulates or unburned fuel is present in the flow stream. Additionally, these devices are typically much smaller and lightweight compared to a vacuum pump, making them potentially easier to integrate into existing experimental setups. There is added flexibility in that the suction flow rate is a function of the motive pressure utilized,

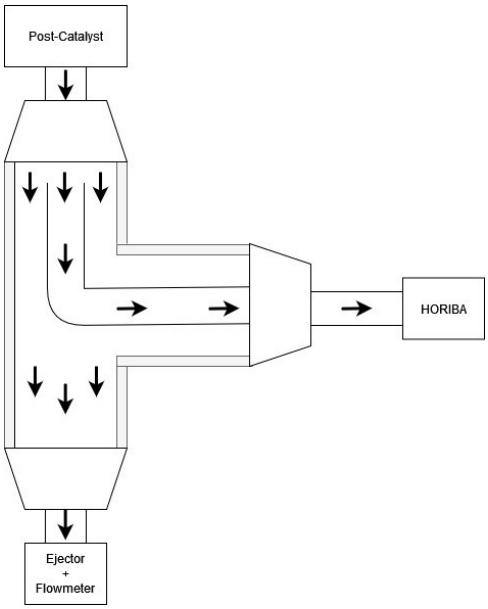

Figure 3: Horiba sampling probe configuration.

which expands the range of possible flow rates that can be evaluated with a single device. The motive pressure acts as a coarse control for the suction flow rate, and the addition of a needle valve inline allows for more fine control of the flow rate.

Integration of either device with an existing sampling system requires additional care. As both devices generate a low pressure zone, if the the suction is strong enough, it may potentially pull flow out of the emissions analyzer. To combat this, we have designed our probe with a 90° bend such that the inlet of the emissions analyzer is 180° from the outlet flow to the ejector as in Figure 3. Furthermore, the HORIBA emissions analyzer's own sample flowrate must be taken into account, as this flow stream passes only through the analyzer and not through the flowmeter. The total flow through the system, $\dot{V}$, is thus the sum of both flow streams as in Eq. (7). Note that the HORIBA analyzer attempts to pull a steady flowrate of up to approximately 5 LPM of exhaust gas, and this parameter will change based on the specific emissions analyzer utilized.

$$\dot{V} = \dot{V}_{flowmeter} + \dot{V}_{HORIBA} \tag{7}$$

Measuring the Secondary Flow

To meet the designated flow considerations, flow through the secondary branch must be able to be measured. Measurement of the secondary flow was performed using an Alicat flowmeter between the outlet of the catalyst and the inlet of the suction line on the ejector. The device is temperature sensitive with a maximum operating temperature of 60 °C, far below the typical exhaust temperatures of 600 °C as well as below the catalyst operating temperature. Thus, the sampling line requires cooling prior to entering the flowmeter to avoid damaging the device. However, cooling alone creates an additional complication: at below 60 °C, the water vapor in the exhaust gas can condense. Since the flowmeter is not designed to handle any condensation, a water trap is necessary to remove any moisture prior to entering the device. To do so, 1.82 m (6 ft) of 6.35 mm (1/4") stainless steel tubing was coiled to act as a heat-exchanger section and fed at an angle into the water trap. The water trap is essentially a large volume with threaded connection points for water to collect within with a flow sight at the top to determine the water level. This large volume is placed inside an ice bath to ensure all the water condenses prior to reaching the flowmeter.

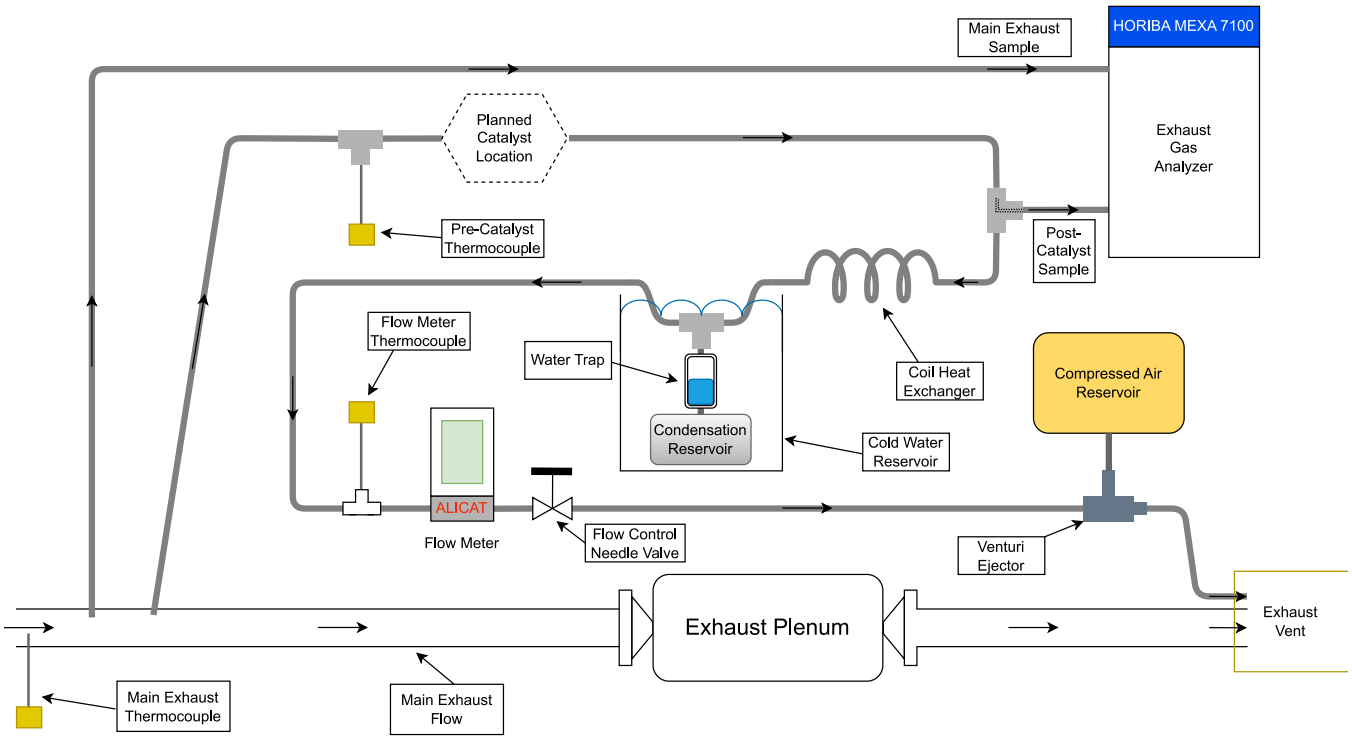

Figure 4: Flow diagram for main and secondary exhaust branches.

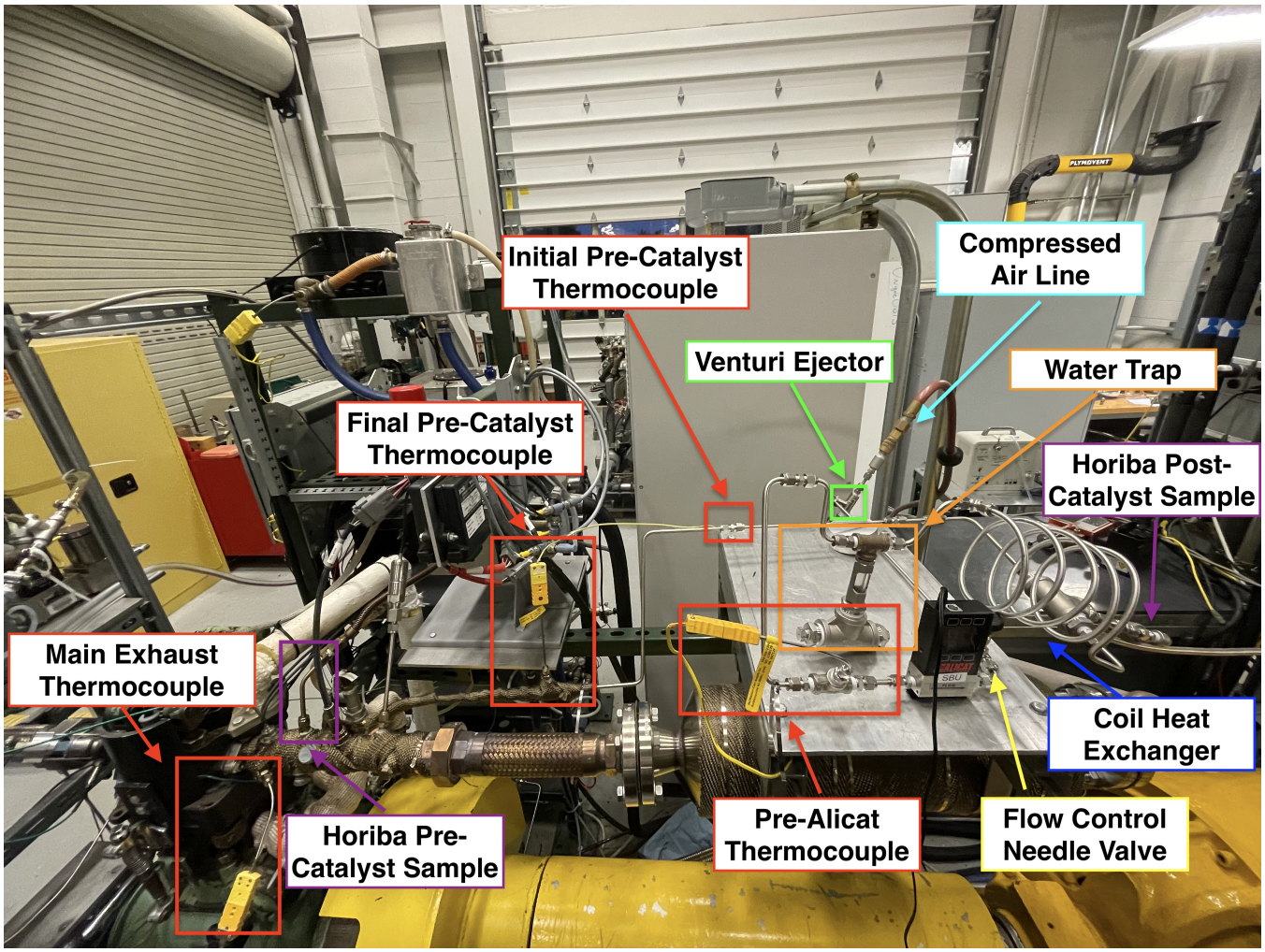

Figure 5: Installed catalyst branch.

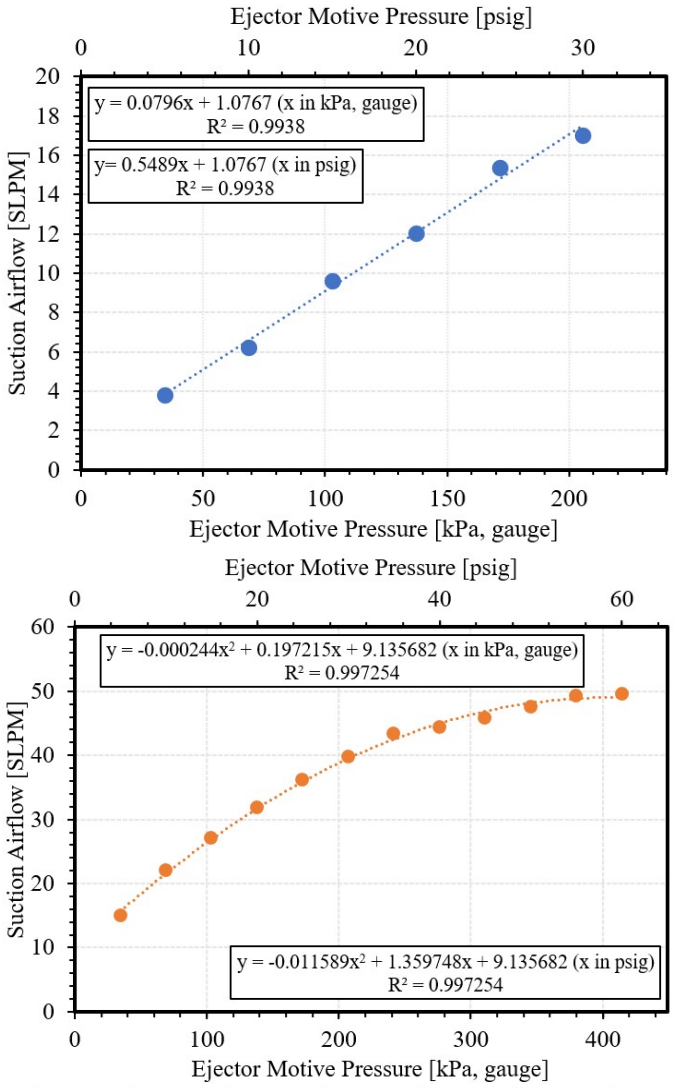

Figure 6: Suction flow solely due to the ejector as a function of compressed air motive gas pressure for -030 (top) and -060 (bottom) ejector models.

Full System Design

The result of the aforementioned design considerations is depicted in Figure 4, with the physical system itself included in Figure 5. Immediately at the main exhaust port, a sample is taken using the HORIBA emissions analyzer and another line is directed towards that catalyst. Temperature measurements are taken at the main exhaust branch, the secondary branch pre-catalyst, and the secondary branch pre-flowmeter. After the sample passes through the catalyst, another HORIBA sampling line pulls the post-catalyst sample for analysis, and the remainder of the flow passes through a coil heat exchanger and water trap. After the trap, it passes through the flow meter and ejector, with the needle valve inline for precise flow control. After passing through the ejector, the mixture is diluted and vented outdoors.

Validation and Testing Data

Flow rate

The total flow rate through the main and secondary branches is first determined via the total available exhaust flow at the given intake pressure and engine speed. The low range limit on the engine speed is dictated by the dynamometer, which should not have extended operation below 500RPM. Additionally, the low range limit of the intake pressure is dictated by whether stable combustion can be achieved at the given engine speed and intake pressure. By lowering both intake pressure and engine speed from normal operating conditions (1200 RPM, 75 kPa) to the lowest values possible (500RPM, 34.5 kPa), the exhaust flow rate was varied between 186.8 SLPM to 24.3 SLPM as shown in Table 2. Thus, the engine operating conditions themselves can be used to make a coarse adjustment in the total outlet flow. This sets an upper limit for how much flow the secondary branch can siphon off from the main branch depending on operating condition. However, the benefit of the secondary branch system is that the system is partially decoupled: there is no lower limit at any engine operating condition. This prevents the engine from needing to be operated under non-realistic conditions to achieve the desired catalyst flow rate.

Table 2: Main Exhaust Flow Characterization

Engine Speed [RPM]	Intake Pressure [kPa]	Main Exhaust Flow Rate[SLPM]
1200	75	186.8
1200	51.5	122
1200	37	81.9
900	51	89.3
900	38	56.3
600	50.5	117
600	43.1	44.1
600	37.9	36.5
600	35	32.1
500	34.5	24.3

Once the upper limit on flow through the secondary branch is determined, the motive pressure on the ejector can be set to get within the desired flow range, and the needle valve adjusted for more fine control. Ideally, the flow through the branch is set knowing the catalyst's required space velocities and its geometric information. Two ejector models were characterized with the needle valve wide open against a sweep of ejector motive pressures as depicted in Figure 6. Ejector models are denoted by their orifice size in thousands of an inch, with the larger orifice size allowing for flows of up to 50 SLPM at the motive pressures tested. However, the larger ejector model utilizes more compressed air, and thus the smaller model was utilized for low flow conditions to minimize compressor cycling.

Branch Temperatures

The engine setup also allows for controlling of the main exhaust temperature by varying operating conditions. Table 3 shows the main exhaust temperature can take on a wide range of values by adjusting the main exhaust flow rate (this can be varied by changing the engine speed and intake pressure) and the spark timing. However, the temperature at the inlet of the catalyst is not only a function of main exhaust temperature, but also the secondary branch tube length, tube diameter, and

Table 3: Main Exhaust Temperature Characterization

Main Exhaust Flow Rate [SLPM]	Spark Timing [deg ATDC]	Main Exhaust Temperature [K]
186.8	-4	860.7
56.3	-18	714.1
36.5	1	672.2
36.5	-4	658.6
36.5	-9	648.1
36.5	-14	624.4
36.5	-19	598.6
36.5	-24	581.6
32.1	-5	637.9
32.1	-10	605.4
32.1	-15	590.7
32.1	-20	577.4

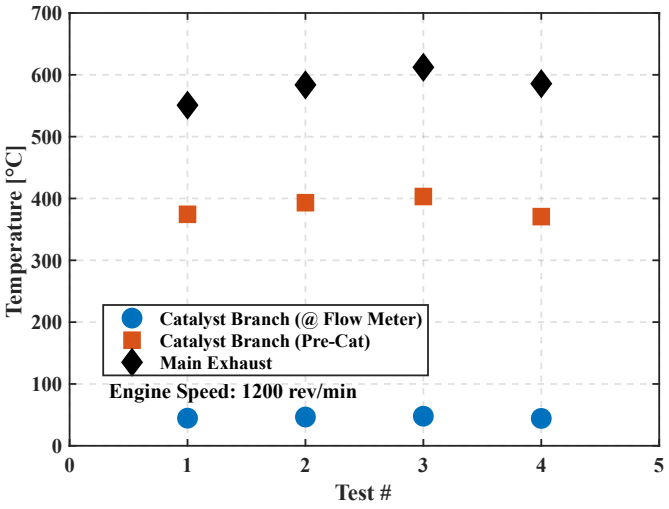

Figure 7: Temperature at key branch locations under various engine operating conditions.

flow rate. As mentioned previously, more heat is lost from the gas stream as the tube length increases and the diameter decreases, which allows these parameters to be used as coarse adjustments for the catalyst branch flow rate. These heat losses are made evident in Figure 7 which shows the temperatures in the main exhaust, catalyst branch just before reaching the catalyst location, and catalyst branch at the inlet of the flowmeter. The temperature pre-catalyst can theoretically take on any value between the main exhaust and the flowmeter by altering the tube geometry. The system is thus modular; additional length of tubing can be coiled and standardized to fit the same footprint, allowing for these coils to be swapped out if a significant temperature difference is required without altering engine operating conditions. While only relatively high pre-catalyst temperatures are discussed herein, the authors note that additional length of tubing was sufficient to bring the pre-catalyst temperature to the 200 — 300 °C range with ease.

If engine operating conditions are able to be altered, the equivalence ratio presents another parameter to significantly alter the main exhaust temperature (and thus the catalyst inlet temperature). This is best depicted in Figure 8, where pure CH_4 is burned from the lean limit to the knock limit. A near 200 °C drop in temperature is achieved by altering only the air-fuel ratio. This, in combination with the aforementioned modular length system, can bring the pre-catalyst temperature

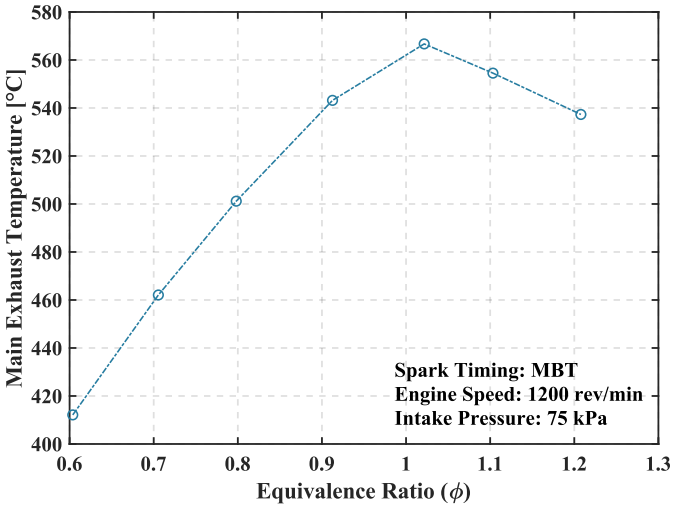

Figure 8: Variation in main exhaust branch temperature as a function of fuel-air equivalence ratio for pure methane combustion.

Table 4: Exhaust Methane Emissions Characterization

Main Exhaust Flow Rate [SLPM]	Spark Timing [deg ATDC]	Exhaust Methane Emissions [ppm]
186.8	-4	1691
56.3	-18	1211
36.5	1	908
36.5	-4	937
36.5	-9	1381
36.5	-14	1953
36.5	-19	3217
36.5	-24	3604
32.1	-5	1162
32.1	-10	2122
32.1	-15	2538
32.1	-20	2995

to within the desired range. The spark timing can then be adjusted to make minor incremental adjustments to match the temperature. This is all achievable without any exterior heat source. If desired, heat tape can be applied to the tubing to provide another dimension of control to the system.

Branch Emissions

Emissions species generated are solely a function of engine operating condition; no additional species should form due to the presence of the secondary branch. This has potential to occur via intermediate reactions due to increased residence time or quenching. In terms of what species may be generated, our testing facility was capable of producing the key emissions species depicted in Figure 9 with the combustion of pure methane. Altering the equivalence ratio at optimal spark timing resulted in CH_4 emissions up to 1653 ppm, NOx emissions up to 3219 ppm, and CO emissions up to 3.7%. Additional variation in the emissions species produced can occur by altering the combustion phasing (spark timing) to produce more or less incomplete combustion byproducts for conversion. This behavior is shown in Table 4, where the spark timing is varied at different exhaust flow rates, leading to significant changes in the CH_4 concentration in the exhaust stream. For a constant exhaust flow rate (36.5 SLPM), varying the spark timing caused the CH_4 emissions to change from 908 ppm to 3604 ppm. This is because the combustion efficiency is heavily affected by the spark timing. A lower combustion efficiency will lead to higher CH_4 emissions as more of the fuel will go from intake to exhaust without participating in the combustion process.

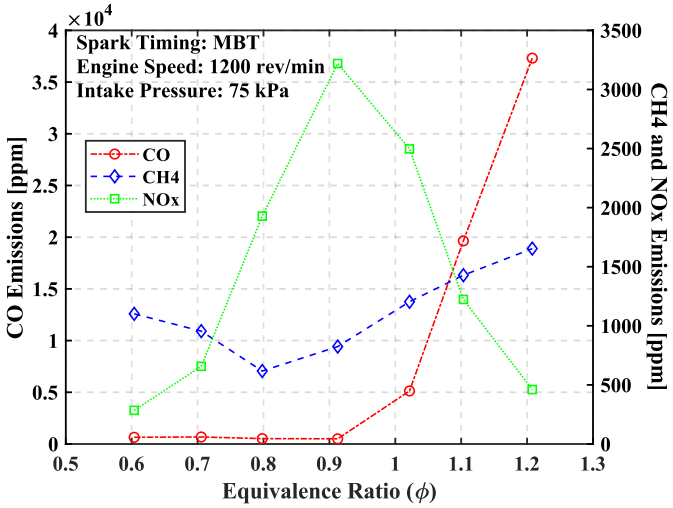

Figure 9: Variation in key emissions species as a function of fuel-air equivalence ratio for pure methane combustion.

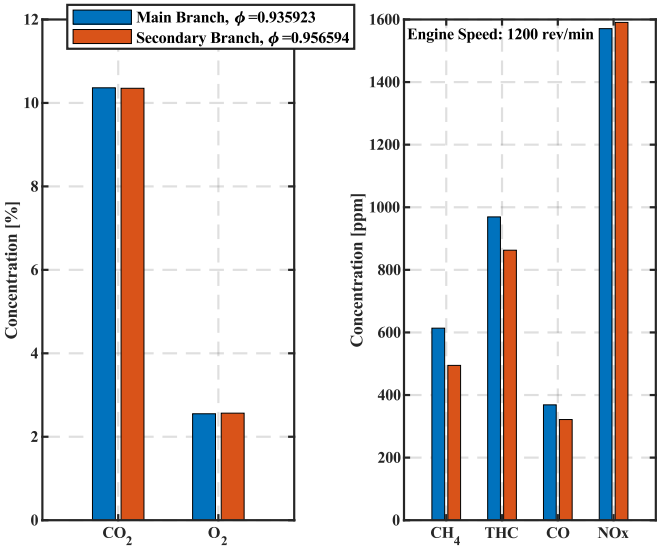

Figure 10: Full emissions profile at main exhaust branch and secondary branch.

To determine the effectiveness of the secondary branch in producing similar emissions to the main branch, a test was performed at slightly lean conditions ($\phi < 1$) relevant to automotive applications as in Figure 10. Two distinct sampling lines are used for the main and secondary branch, each leading to its own heated filter. After the heated filter, the two sampling lines feed their respective sample gas into the main analyzer flow path where an internal diverting valve is used to manually switch between the sample lines. As only one branch sample stream is measured at a given instant under steady-state flow conditions, the same flow path is used for both sample lines post diverting valve. The sampled gas is then split into multiple internal flow paths, where each emissions species is separately measured. When validating the system, oxygen (O_2) readings may be used as one indicator of a leak, as air is sucked into the system and the dilution results in an increase in measured O_2. Emissions species O_2, carbon dioxide (CO_2) and nitrogen oxides (NOx) were consistent between the secondary branch and the main exhaust, indicating that there is no leak entering the analyzer on either sampling line. In terms of incomplete combustion products, namely CH_4, total hydrocarbons (THC), and CO, differences on the order of the analyzer's uncertainty were observed. The uncertainty in emissions species is $\pm$ 1 % of full scale, which results in an uncertainty of 100 ppm, 30 ppm, and 50 ppm for THC, CH_4, and CO, respectively. Changes in time-of-flight on each sampling path due to sample location and length deviations may also result in small yet measurable differences in species concentration, and thus these differences should be minimized if at all possible. Thus, the secondary branch produced a representative emissions profile when compared to the main branch, indicating the ability to provide the aftertreatment device with a realistic flow stream characteristic of the operating conditions used.

Range of System Capabilities

The slip-stream sampling system as a whole presents a wide range of possible flowrates, temperatures, and emission species that may be used to further aftertreatment device characterization and development. The system is modular, allowing for different aftertreatment devices to be installed with minimal alteration to the system. Achieving the required catalyst conditions is possible through altering the equivalence ratio, intake pressure, fuel type, spark timing, engine speed, tubing length, and ejector motive pressure. The engine can be throttled to alter the intake pressure and the engine speed adjusted to produce main exhaust flowrates anywhere between 32.1 – 186.8 SLPM, which sets the global upper limit of what is achievable in the secondary branch during operation. In practice, the achievable upper limit is dictated by the suction flow the ejector is capable of producing as the motive pressure is adjusted, with the current model able to produce suction flows up to 50 SLPM. The minimal flow through the secondary branch is dictated by the HORIBA emissions analyzer, which pulls approximately up to 5 SLPM and results in an effective range of 5 – 50 SLPM in the secondary branch. This flexibility is critical, as the variable flowrate allows for variably-sized mini-core catalysts to be utilized while maintaining the required $GHSV$ for testing. This reduces the amount of material and time required to produce the catalyst before it can be tested in a realistic engine environment. In terms of temperatures, the equivalence ratio, intake pressure, and spark timing can be adjusted to change the main exhaust branch temperature, which is able to achieve temperatures between 306 – 612 °C. The secondary branch temperature is a function of the main exhaust branch temperature, tube geometry, and flowrate utilized, and is currently able to achieve between 55 – 400 °C . Further additions, such as larger diameter tubing and heat tape, may allow for the upper temperature limit to be extended to that of the main branch. Emissions delivered to both the main and secondary branches are function of the combustion efficiency, which is a function of the spark timing and equivalence ratio. The system has been shown to be able to produce unburned CH_4 emissions between 617 – 3604 ppm, NOx emissions between 284 – 3219 ppm, and CO emissions between 0.06 – 3.7%. Higher emissions are able to be produced, but go beyond the extent of our system's emissions analyzer. While simulated exhaust gas through the use of heating and bottle gas could be utilized to produce this range, it does not reap the benefits of real species emissions generation in the system, which better reflects real-world operation. Thus, the systems' overall flexibility and wide range of operating points allows it to be utilized for testing a variety of different aftertreatment device configurations.

Conclusions

In summary, a single-cylinder CFR engine was used to produce emissions species to develop and test a secondary slip-stream sampling system. A range of engine operating conditions were investigated to understand the extent of the system's capabilities. The key findings demonstrated in this work can be briefly described by the following remarks:

- An exhaust Reynolds number of 4767.7 indicates turbulence, which has been found in prior literature to be sufficient to assume the exhaust gases are well-mixed for unbiased sampling.
- Aftertreatment devices have specific requirements in terms of $GHSV$, and scaling down the flowrate allows for a similarly scaled down catalyst.
- Consideration to other instrumentation in the sampling section is necessary, and the addition of a water trap may be required depending on individual system requirements if the operating temperature range is below the dew-point of the exhaust gas stream.
- Exhaust temperatures achieved were up to 612 °C in the main exhaust and 400 °C in the secondary branch through varying engine operating conditions, such as equivalence ratio, intake pressure, spark timing, and tubing characteristics.
- The geometric characteristics (diameter/length) of initial section of the secondary branch as it leaves the main branch impact the upper temperature limit the secondary branch can achieve. A temperature gradient of 4.92 °C/cm (150 °C/ft) with 6.35 mm (1/4") stainless steel tubing was noted, with potential to decrease heat losses through the use of larger diameter tubing or heat tape.
- The sampling system is partially decoupled from the engine operating conditions, which result in 32.1 – 186.8 SLPM of total flow, allowing for a prescribed flowrate between 5 – 50 SLPM through the aftertreatment device accomplished via a venturi ejector.
- It was demonstrated that the sampling method applied in this work enables the sampling of gases into the catalyst branch with a chemical composition substantially similar to that of the gases in the main exhaust flow, which range between 617 and 3604 ppm for unburned methane.
- The developed system demonstrated the ability to achieve a wide range of flows, temperatures, and gas compositions through the catalyst by separately adjusting engine operating conditions as well as the physical characteristics of the secondary branch.

- The system is modular and upgradeable, allowing for the installation of different geometric tubing characteristics and temperatures to meet different catalyst requirements.

In essence, the system's flexibility allows for scaled-down testing of aftertreatment devices under realistic engine operating conditions, which reduces the amount of production time and material required to test the aftertreatment device.

References

1. Lattanzio, R. K. *et al.*, "U.S. Climate Change Policy," Congressional Research Service (CRS), Tech. Rep., Oct. 2021, pp. 1–43. [Online]. Available: https://crsreports.congress.gov/product/pdf/R/R46947.
2. Horowitz, C. A., "Paris Agreement," *International Legal Materials*, vol. 55, no. 4, pp. 740–755, Aug. 2016, ISSN: 0020-7829. DOI: 10.1017/S0020782900004253.
3. Kasab, J. and Strzelec, A., *Automotive Emissions Regulations and Exhaust Aftertreatment Systems*. SAE International, 2020.
4. Keenan, M., "Exhaust Emissions Control: 60 Years of Innovation and Development," SAE Technical Paper 2017-24-0120, Sep. 2017. DOI: 10.4271/2017-24-0120.
5. Blakeman, P. G., Chiffey, A. F., Phillips, P. R., Twigg, M. V., and Walker, A. P., "Developments In Diesel Emission Aftertreatment Technology," SAE Technical Paper 2003-01-3753, Nov. 2003. DOI: 10.4271/2003-01-3753.
6. Guan, B., Zhan, R., Lin, H., and Huang, Z., "Review of state of the art technologies of selective catalytic reduction of NOx from diesel engine exhaust," *Applied Thermal Engineering*, vol. 66, no. 1-2, pp. 395–414, May 2014, ISSN: 13594311. DOI: 10.1016/j.applthermaleng.2014.02.021.
7. Ni, P., Wang, X., and Li, H., "A review on regulations, current status, effects and reduction strategies of emissions for marine diesel engines," *Fuel*, vol. 279, p. 118 477, Nov. 2020, ISSN: 00162361. DOI: 10.1016/j.fuel.2020.118477.
8. Maricq, M. M., "Engine, aftertreatment, fuel quality and non-tailpipe achievements to lower gasoline vehicle PM emissions: Literature review and future prospects," *Science of The Total Environment*, vol. 866, p. 161 225, Mar. 2023, ISSN: 00489697. DOI: 10.1016/j.scitotenv.2022.161225.
9. Zhang, Z. *et al.*, "The development of diesel oxidation catalysts and the effect of sulfur dioxide on catalysts of metal-based diesel oxidation catalysts: A review," *Fuel Processing Technology*, vol. 233, p. 107 317, Aug. 2022, ISSN: 03783820. DOI: 10.1016/j.fuproc.2022.107317.
10. Kašpar, J., Fornasiero, P., and Hickey, N., "Automotive catalytic converters: current status and some perspectives," *Catalysis Today*, vol. 77, no. 4, pp. 419–449, Jan. 2003, ISSN: 09205861. DOI: 10.1016/S0920-5861(02)00384-X.
11. Pai, D. and Prabhu, M. K., "Recent Advances in Substrate Materials and Thermal Analysis of Catalytic Converters," *Materials Today: Proceedings*, vol. 5, no. 11, pp. 24 221–24 230, 2018, ISSN: 22147853. DOI: 10.1016/j.matpr.2018.10.217.
12. Weisweiler, W. and Wunsch, R., "Simulation of a driving cycle in laboratory: an approach for testing catalysts suitable for automotive exhaust NOx abatement under lean conditions," *Chemical Engineering and Processing: Process Intensification*, vol. 37, no. 3, pp. 229–232, May 1998, ISSN: 02552701. DOI: 10.1016/S0255-2701(98)00027-0.
13. Burkholder, S. and Cooper, B. J., "Effect of Aging and Testing Conditions on Catalyst Performance," in *Automotive Industry in Expanding Countries Conference Proceedings*, SAE Technical Paper 911734, Sep. 1991. DOI: 10.4271/911734.
14. Casassa, J. P. and Beyerlein, D. G., "Engine Dynamometers for the Testing of Catalytic Converter Durability," SAE Technical Paper 730558, Feb. 1973. DOI: 10.4271/730558.
15. Haslett, R. A., "A Technique for Endurance Testing of Oxidation Catalytic Reactors," in *1974 Automotive Engineering Congress and Exposition*, SAE Technical Paper 740246, Feb. 1974. DOI: 10.4271/740246.
16. Boruc, L. *et al.*, "An Experimental Facility for Rapid Testing of SCR Systems," SAE Technical Paper 2020-01-2192, Sep. 2020. DOI: 10.4271/2020-01-2192.
17. Moulijn, J. A., Perez-Ramirez, J., Diepen, A. van, Kreutzer, M. T., and Kapteijn, F., "Catalysis Engineering on Three Levels," *International Journal of Chemical Reactor Engineering*, vol. 1, no. 1, Sep. 2003, ISSN: 1542-6580. DOI: 10.2202/1542-6580.1093.
18. Wu, C. T., Yameogo, A., and Lu, J.-H., "Using Bypass to Simulate the Deterioration of Catalyst in a Motorcycle Engine," SAE Technical Paper 2013-01-0048, Mar. 2013. DOI: 10.4271/2013-01-0048.
19. Aardahl, C. L., Rappé, K. G., Park, P. W., Ragle, C. S., Boyer, C. L., and Faulkner, S. A., "Steady-State Engine Testing of γ-Alumina Catalysts Under Plasma Assist for NOx Control in Heavy-Duty Diesel Exhaust," SAE Technical Paper 2003-01-1186, Mar. 2003. DOI: 10.4271/2003-01-1186.
20. Twomey, S., *Developments in Atmospheric Science, 7: Atmospheric Aerosols*. Amsterdam: Elsevier Scientific Publishing Company, 1977.
21. Davidson, T. A., "Simple and accurate method for calculating viscosity of gaseous mixtures," Centers for Disease Control and Prevention, Tech. Rep., 1993.
22. Rood, S., Eslava, S., Manigrasso, A., and Bannister, C., "Recent advances in gasoline three-way catalyst formulation: A review," *Proceedings of the Institution of Mechanical Engineers, Part D: Journal of Automobile Engineering*, vol. 234, no. 4, pp. 936–949, Mar. 2020, ISSN: 0954-4070. DOI: 10.1177/0954407019859822.
23. Eckhardt, B., Schneider, T. M., Hof, B., and Westerweel, J., "Turbulence Transition in Pipe Flow," *Annual Review of Fluid Mechanics*, vol. 39, no. 1, pp. 447–468, Jan. 2007, ISSN: 0066-4189. DOI: 10.1146/annurev.fluid.39.050905.110308.
24. P. Kulkarni, P. A. Baron, and K. Willeke, Eds., *Aerosol Measurement*. Wiley, Jun. 2011, ISBN: 9780470387412. DOI: 10.1002/9781118001684.
25. Kayes, D. and Hochgreb, S., "Mechanisms of Particulate Matter Formation in Spark-Ignition Engines. 1. Effect of Engine Operating Conditions," *Environmental Science & Technology*, vol. 33, no. 22, pp. 3957–3967, Nov. 1999, ISSN: 0013-936X. DOI: 10.1021/es9810991.
26. Breugel, J. W. van, Stein, J. J. M., and Vries, R. J. de, "Isokinetic Sampling in a Dense Gas-Solids Stream," *Proceedings of the Institution of Mechanical Engineers, Conference Proceedings*, vol. 184, no. 3, pp. 18–23, Sep. 1969, ISSN: 0367-8849. DOI: https://doi.org/10.1243/PIME_CONF_1969_184_075_02.
27. Rappé, K. G. *et al.*, "Aftertreatment Protocols for Catalyst Characterization and Performance Evaluation: Low-Temperature Oxidation, Storage, Three-Way, and NH3-SCR Catalyst Test Protocols," *Emission Control Science and Technology*, vol. 5, no. 2, pp. 183–214, Jun. 2019, ISSN: 2199-3629. DOI: 10.1007/s40825-019-00120-7.
28. Petrov, A. W., Ferri, D., Tarik, M., Kröcher, O., and Bokhoven, J. A. van, "Deactivation Aspects of Methane Oxidation Catalysts Based on Palladium and ZSM-5," *Topics in Catalysis*, vol. 60, no. 1-2, pp. 123–130, Feb. 2017, ISSN: 1022-5528. DOI: 10.1007/s11244-016-0724-6.
29. Gélin, P. and Primet, M., "Complete oxidation of methane at low temperature over noble metal based catalysts: a review," *Applied Catalysis B: Environmental*, vol. 39, no. 1, pp. 1–37, Nov. 2002, ISSN: 09263373. DOI: 10.1016/S0926-3373(02)00076-0.

30. Heck, R. M., Gulati, S., and Farrauto, R. J., "The application of monoliths for gas phase catalytic reactions," *Chemical Engineering Journal*, vol. 82, no. 1-3, pp. 149–156, Mar. 2001, ISSN: 13858947. DOI: 10.1016/S1385-8947(00)00365-X.

31. Geus, J. W. and Giezen, J. C. van, "Monoliths in catalytic oxidation," *Catalysis Today*, vol. 47, no. 1-4, pp. 169–180, Jan. 1999, ISSN: 09205861. DOI: 10.1016/S0920-5861(98)00297-1.

32. Ferrizz, R. M., Stuecker, J. N., Cesarano, J., and Miller, J. E., "Monolithic Supports with Unique Geometries and Enhanced Mass Transfer," *Industrial & Engineering Chemistry Research*, vol. 44, no. 2, pp. 302–308, Jan. 2005, ISSN: 0888-5885. DOI: 10.1021/ie049468r.

33. Govender, S. and Friedrich, H., "Monoliths: A Review of the Basics, Preparation Methods and Their Relevance to Oxidation," *Catalysts*, vol. 7, no. 12, p. 62, Feb. 2017, ISSN: 2073-4344. DOI: 10.3390/catal7020062.

34. Vergunst, T., Kapteijn, F., and Moulijn, J. A., "Optimization of Geometric Properties of a Monolithic Catalyst for the Selective Hydrogenation of Phenylacetylene," *Industrial & Engineering Chemistry Research*, vol. 40, no. 13, pp. 2801–2809, Jun. 2001, ISSN: 0888-5885. DOI: 10.1021/ie000712y.

35. Loprete, J., Ristow Hadlich, R., Sirna, A., Shaalan, A., and Assanis, D., "Combustion Performance and Emissions Characterization of Methane-Hydrogen Blends (Up to 50% by vol.) in a Spark-Ignited Cfr Engine," in *Internal Combustion Engine Division Fall Technical Conference*, Technical Paper ICEF2023-110538, 2023.

36. Ran, Z., Longtin, J., and Assanis, D., "Investigating anode off-gas under spark-ignition combustion for SOFC-ICE hybrid systems," *International Journal of Engine Research*, vol. 23, no. 5, pp. 830–845, May 2022, ISSN: 1468-0874. DOI: 10.1177/14680874211016987.

37. Ran, Z., Assanis, D., Hariharan, D., and Mamalis, S., "Experimental Study of Spark-Ignition Combustion Using the Anode Off-Gas from a Solid Oxide Fuel Cell," SAE Technical Paper 2020-01-0351, Apr. 2020. DOI: 10.4271/2020-01-0351.

38. Ran, Z., Hariharan, D., Lawler, B., and Mamalis, S., "Experimental study of lean spark ignition combustion using gasoline, ethanol, natural gas, and syngas," *Fuel*, vol. 235, pp. 530–537, Jan. 2019, Technical Paper 2020-01-0351, ISSN: 00162361. DOI: 10.1016/j.fuel.2018.08.054.

39. Shaalan, A., Nasim, M. N., Mack, J. H., Van Dam, N., and Assanis, D., "Understanding Ammonia/Hydrogen Fuel Combustion Modeling in a Quiescent Environment," in *ASME 2022 ICE Forward Conference*, American Society of Mechanical Engineers, Oct. 2022, ISBN: 978-0-7918-8654-0. DOI: 10.1115/ICEF2022-91185.

40. Assanis, D., Engineer, N., Neuman, P., and Wooldridge, M., "Computational Development of a Dual Pre-Chamber Engine Concept for Lean Burn Combustion," SAE Technical Paper 2016-01-2242, Oct. 2016. DOI: 10.4271/2016-01-2242.

41. Bergmann, M., Vogt, R., Szente, J., Maricq, M., and Benter, T., "Using Ejector Diluters to Sample Vehicle Exhaust at Elevated Pressures and Temperatures," *SAE International Journal of Engines*, vol. 1, no. 1, pp. 2008–01, Oct. 2008, ISSN: 1946-3944. DOI: 10.4271/2008-01-2434.

42. Swanson, J. J., Watts, W., and Kittelson, D., "Diesel Exhaust Aerosol Measurements Using Air-Ejector and Porous Wall Dilution Techniques," *SAE International Journal of Engines*, vol. 4, no. 1, pp. 2011–01, Apr. 2011, ISSN: 1946-3944. DOI: 10.4271/2011-01-0637.

43. Giechaskiel, B., Ntziachristos, L., and Samaras, Z., "Calibration and modelling of ejector dilutors for automotive exhaust sampling," *Measurement Science and Technology*, vol. 15, no. 11, pp. 2199–2206, Nov. 2004, ISSN: 0957-0233. DOI: 10.1088/0957-0233/15/11/004.

44. Giechaskiel, B., Ntziachristos, L., and Samaras, Z., "Effect of ejector dilutors on measurements of automotive exhaust gas aerosol size distributions," *Measurement Science and Technology*, vol. 20, no. 4, p. 045 703, Apr. 2009, ISSN: 0957-0233. DOI: 10.1088/0957-0233/20/4/045703.

Contact Information

Prof. Dimitris Assanis
(dimitris.assanis@stonybrook.edu)
Assistant Professor
Dept. of Mechanical Engineering
Stony Brook University
131 Light Engineering
100 Nicolls Rd
Stony Brook, NY 11794
USA

Acknowledgments

This work was enabled by funding received from the Alliance for Sustainable Energy, LLC, Managing and Operating Contractor for the National Renewable Energy Laboratory for the U.S. Department of Energy under Subcontract No. NHQ-9-82305-02. We would also like to thank Mike Bunce of MAHLE Powertrain for insightful discussions.

Definitions, Acronyms, Abbreviations

Re	Reynolds Number
ρ	Density
V	Average Velocity
D	Exhaust Diameter
μ	Dynamic Viscosity
y_i	Mole Fraction of Species i
$SLPM$	Standard Liter per Minute
ID	Inner Tube Diameter
OD	Outer Tube Diameter
$\dot{V}$	Volume Flow Rate
$V_{monolith}$	Volume of Catalyst Monolith
$WHSV$	Weight Hourly Space Velocity
$GHSV$	Gas Hourly Space Velocity
c_p	Specific Heat at Constant Pressure
L	Length of Sampling Section
T_{in}	Temperature at Sampling Section Inlet
T_{out}	Temperature at Sampling Section Outlet
$\dot{q}_{loss}$	Heat Loss per Unit Length of Sampling Section